Progress in Earth and Planetary Science

RESEARCH ARTICLE Open Access

Future dynamic sea level change in the western subtropical North Pacific associated with ocean heat uptake and heat redistribution by ocean circulation under global warming

Tatsuo Suzuki* and Hiroaki Tatebe

Abstract

In the present study, the relative importance of ocean heat uptake and heat redistribution on future sea level changes in the western North Pacific has been reconciled based on a set of climate model experiments in which anomalous surface fluxes of wind stress, heat, and freshwater in a warmed climate are separately given to those fluxes in a pre-industrial control simulation. Our findings suggest that the basin-wide ocean heat uptake and resultant heat accumulation by the climatological-mean advection are required to explain the future dynamic sea level (DSL) rise in the western subtropical North Pacific caused by the thermal expansion of subtropical mode water (STMW). At the same time, it has been recognized that the localized heat uptake in association with the wintertime mixed-layer formation around the Kuroshio Extension can be solely attributed to the future STMW change. The thermally induced component is a dominant contribution to the future DSL rise in the western subtropical North Pacific compared to the contributions of wind-induced and halosteric components, which, especially the former, have been reported as a dominant factor resulting from a linear response of the ocean to the northward shift and strengthening of the mid-latitude westerly over the North Pacific in a warmed climate.

Keywords: Sea level, Global warming, Heat uptake, North Pacific

1 Introduction

The global ocean stores more than 90% of the heat energy accumulated in the climate system of the Earth during recent decades (e.g., Levitus et al. 2012; Church et al. 2013a, b). Whereas the ocean heat uptake works to reduce abrupt global warming, the thermal expansion of seawater causes sea level rise, which has been recognized as a severe societal issue due to future global warming (Willis and Church 2012). The ongoing global mean sea level rise will continue in the future few centuries depending on future greenhouse gas emissions, even when the greenhouse gas concentration is stabilized (Church et al. 2013a, b). In addition, regional sea level changes will significantly deviate from global mean values. For coastal and small island countries, the territorial sea level rise can be substantially more important than the global mean (Cazenave and Cozannet 2014). The complete regional sea level changes are characterized by many processes involving the ocean, the atmosphere, the geosphere, and the cryosphere. Dynamical ocean response, which can be represented in global atmosphere-ocean general circulation models (AOGCMs), is an essential factor.

The dynamic sea level (DSL) is defined as the deviation from the ocean geoid (e.g., Zhang et al. 2014;

* Correspondence: tsuzuki@jamstec.go.jp
Japan Agency for Marine-Earth Science and Technology, 3173-25 Showa-machi, Kanazawa-ku, Yokohama, Kanagawa 236-0001, Japan

Springer Open

© The Author(s). 2020 **Open Access** This article is licensed under a Creative Commons Attribution 4.0 International License, which permits use, sharing, adaptation, distribution and reproduction in any medium or format, as long as you give appropriate credit to the original author(s) and the source, provide a link to the Creative Commons licence, and indicate if changes were made. The images or other third party material in this article are included in the article's Creative Commons licence, unless indicated otherwise in a credit line to the material. If material is not included in the article's Creative Commons licence and your intended use is not permitted by statutory regulation or exceeds the permitted use, you will need to obtain permission directly from the copyright holder. To view a copy of this licence, visit http://creativecommons.org/licenses/by/4.0/.

Griffies et al. 2016). The geographical pattern of the projected DSL change under global warming can be attributed to changes in ocean density and circulation (e.g., Lowe and Gregory 2006; Suzuki and Ishii 2011). In the present study, we focus on the heat uptake and the DSL change in the western subtropical North Pacific. The DSL changes in the western North Pacific are characterized by a northward shift of the Kuroshio Extension (KE) path and strengthening of the Kuroshio and the KE recirculation gyre. These characteristic patterns are observed in the multi-model ensemble mean of the Coupled Model Intercomparison Project (CMIP) models (e.g., Sueyoshi and Yasuda 2012; Zhang et al. 2014; Yin 2012; Church et al. 2013a, b; Terada and Minobe 2018). Sueyoshi and Yasuda (2012) showed that models with a northward shift of the KE exhibit a poleward shift of the Aleutian Low. Zhang et al. (2014) also inferred that the poleward displacement of the mid-latitude westerly wind causes the poleward expansion of the subtropical gyre in the upper ocean. This is consistent with downscaling experiments using the ocean circulation model by Liu et al. (2016). However, changes in the surface wind stress alone cannot fully explain the strengthening of the KE recirculation.

Analyzing CMIP5 models, Terada and Minobe (2018) suggested that the strengthening of the KE under global warming can be caused by enhanced meridional pressure gradient associated with thermal expansion of subtropical mode water (STMW) and corresponding steric sea level rise in the KE recirculation. Two earlier studies using different climate models suggested that the ocean heat uptake due to the global warming causes thermosteric sea level rise in this region (Lowe and Gregory 2006; Suzuki and Ishii 2011). They estimated the effect of heat flux as the residual of overall change under global warming minus the contribution of changes in the wind stress and the freshwater flux. Therefore, influences of the surface heat flux and resultant ocean heat uptake on future sea level changes are not directly quantified. Furthermore, Terada and Minobe (2018) inferred that the decrease of STMW density is induced by the downward heat flux anomaly related to the northward shift of the KE, which is caused by wind stress change. However, the relationship between the ocean heat uptake and the DSL rise in the Kuroshio and the KE recirculation gyre remains unclear.

In the present study, we use the sixth version of the Model for Interdisciplinary Research on Climate (hereinafter, MIROC6) to investigate the future DSL change in the western subtropical North Pacific. In order to clarify the causes of regional variations, we conducted idealized experiments following Gregory et al. (2016). Furthermore, we focus on the contributions of the ocean heat uptake and heat redistribution by ocean circulation on the DSL change in order to understand the physical nature of the relative sea level rise in the KE recirculation.

2 Methods

The climate model used in the present study, MIROC6, has been cooperatively developed by the Japanese modeling community (Tatebe et al. 2019). The atmospheric component has a horizontal resolution of a T85 spectral truncation with 81 vertical levels. The ocean component has a tri-polar horizontal coordinate system with a nominal resolution of 1° with 62 vertical levels. The pre-industrial control experiment (piControl) reasonably simulated the climatological values of the oceanic environment corresponding to major ocean gyres. Because of limited computational resources, we also used MIROC5.2, which has a lower resolution atmospheric component (T42 spectral truncation with 40 vertical levels) with different physical parameterizations, whereas the ocean component of this model is the same as in MIROC6 (Tatebe et al. 2018). MIROC5.2 has a lower computational cost than MIROC6, allowing more ensemble experiments to be performed.

We conducted a series of idealized model experiments for detailed analysis of the DSL change and the ocean heat uptake in the North Pacific, following the procedure provided by the Flux-Anomaly-Forced Model Intercomparison Project (FAFMIP; Gregory et al. 2016). In the FAFMIP experiments, a prescribed set of surface flux perturbations (shown in the upper panels of Fig. 1) is additionally given to the ocean component of the climate model during a pre-industrial control simulation. These perturbations are defined as the difference between the climatological monthly time mean of years 61–80 of the 1% per year CO_2 concentration increase experiments of CMIP5 (hereinafter, 1pct CO_2 experiment) when the atmospheric CO_2 concentration becomes approximately double and the climatological monthly time mean of the corresponding 20 years of piControl in the CMIP5-MME (multi-model ensemble mean; Gregory et al. 2016). Anomalous ocean heat uptake into the North Pacific (Fig. 1b) is approximately 145 TW, approximately 20% of the global ocean heat uptake. In the North Pacific, the features of the prescribed flux perturbations of CMIP5-MME (Fig. 1 a though c), such as the northward shift of the Aleutian Low, are substantially the same as the flux changes observed in the 1pct CO_2 experiments of MIROC6 and MIROC5.2 (not shown).

The lower panels of Fig. 1 show the DSL changes for the CMIP5-MME, MIROC6, and MIROC5.2 in the 1pct CO_2 experiment relative to each control experiment. The CMIP5-MME shows the characteristics of the DSL distribution associated with the climatological North Pacific circulation (contours in Fig. 1d). We can see the remarkable meridional slope of the mean DSL between 32° N and 38° N, which corresponds to the KE. A similar meridional slope is also found in MIROC6 (Fig. 1e) and MIROC5.2 (Fig. 1f), although the slope is much steeper. In the 1pct CO_2 experiment, the DSL

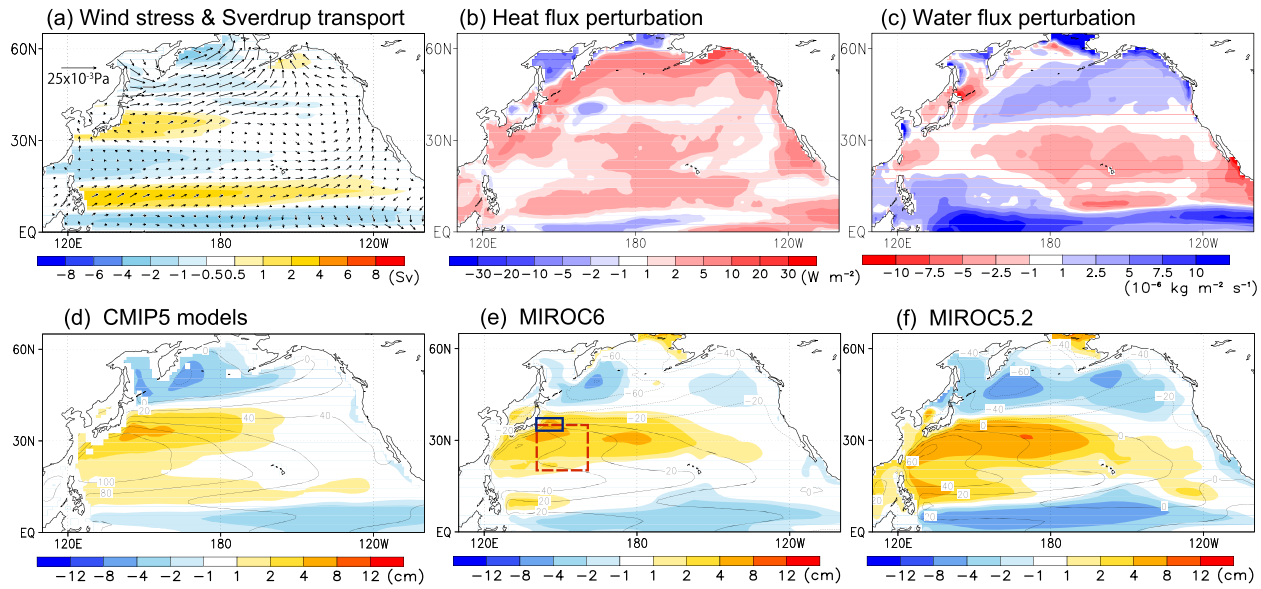

Fig. 1 Imposed surface flux perturbations in the North Pacific for **a** wind stress (arrows), **b** downward heat flux, and **c** downward water flux. These values are anomalies computed from the time mean of years 61–80 in the 1pct CO_2 experiment relative to climatology in piControl. In **a**, colors indicate the stream function of the Sverdrup transport. The lower panels show the dynamic sea level changes of **d** the CMIP5 multi-model ensemble, **e** MIROC6, and **f** MIROC5.2. Time-averages are taken in years 61–80 of the 1pct CO_2 experiments for CMIP5-MME and in years 51–90 for MIROC6 and MIROC5.2. Note that the basin average in the North Pacific is subtracted from the dynamic sea level change at each grid. Contours indicate piControl climatology. Dashed red and solid blue rectangles in **e** indicate the Kuroshio Extension recirculation (20° N–35° N, 140° E–160° E) and the Kuroshio Extension (33° N–37° N, 140° E–150° E) defined in the present study, respectively

rises along the KE, and south of the KE is commonly seen in CMIP5-MME, MIROC6, and MIROC5.2. In order to investigate what physical processes caused these changes, we focus the KE and KE recirculation regions defined as the solid blue (33° N–37° N, 140° E–150° E) and dashed red (20° N–35° N, 140° E–160° E) rectangles in Fig. 1e.

The designated climate experiment in which only the surface wind-stress perturbations are given additionally to the pre-industrial control simulation of MIROC6 is referred to as the faf-stress experiment. Similarly, the climate model experiment in which the surface heat (freshwater) flux perturbation is given is referred to as the faf-heat (faf-water) experiment. In the faf-heat experiment, the net heat flux into the ocean component is $Q = Q_{SST} + F$, where Q_{SST} is the net surface heat flux computed in the climate model, and F is the prescribed heat flux perturbation (Fig. 1b). Note that changes in the sea surface temperature (SST) due to the given surface heat flux perturbation (F) could induce resultant surface heat flux to compensate for the SST change, reducing the total heat input. In order to avoid this negative feedback, two additional tracers of added heat (T_A) and redistributed heat (T_R) are introduced in the faf-heat experiment (Bouttes et al. 2014; Method B in Gregory et al. 2016). Here, T_A, the initial values of which are globally zero, is prognosed as an ocean tracer forced by F, and T_R, the initial condition of which is taken from the ocean temperature of piControl, is also prognosed as an ocean tracer forced by Q_{SST}. The surface heat flux Q_{SST} is estimated using the SST contained in T_R. The ocean potential temperature, θ, which is the sum of T_A and T_R, is integrated with Q. That is to say that the surface heat flux perturbation, F, works to change the ocean temperature and density, and thus the thermosteric height and ocean circulation. In the passive-heat experiment, T_A is also installed in piControl as a passive tracer and integrated with F. Each FAFMIP experiment is performed with a single ensemble simulation in MIROC6 and with three-member ensemble simulations in MIROC5.2. Although 70 year-long integration is required in the FAFMIP protocol, in MIROC6, we extended the integration period to 90 years in order to observe the DSL response to the external forcing, separate from internal variabilities.

Several diagnostic variables are shown in the present study. In order to evaluate the effect of wind stress changes on the basin-scale circulation field, we compute the Sverdrup transport from the wind stress changes. The stream function was derived by integrating the Sverdrup transport from the east coast at each latitude, as follows:

$$\psi(x) = -\frac{1}{\beta}\int_{x}^{xe} \nabla \times \boldsymbol{\tau} dx \qquad (1)$$

where ψ is the stream function of the Sverdrup transport, β is the meridional differentiation of Coriolis

parameter, *xe* is the longitude of the east coast, and $\boldsymbol{\tau}$ is the wind-stress vector.

In order to investigate the DSL change due to the heat input into the ocean, we have estimated thermosteric sea level change as follows:

$$\Delta\eta_\theta = \int_0^H \alpha \times \Delta\theta dz = \int_0^H \alpha \times \Delta T_R dz + \int_0^H \alpha \times T_A dz \quad (2)$$

where α is the coefficient of the thermal expansion, $\Delta\theta$ is the potential temperature difference relative to the climatology of the piControl, and H is ocean depth. In the faf-heat experiment, the thermosteric sea level change ($\Delta\eta_\theta$) is separated into the components due to the redistributed heat change ($\Delta\eta_{TR}$) and the components due to the added heat ($\Delta\eta_{TA}$), as shown in the right-hand side of Eq. (2). In the passive-heat experiment, we estimate $\Delta\eta_{TA}$, which does not affect the DSL or ocean circulation.

Note that we have subtracted the North Pacific basin average from the raw sea level changes at each grid point in order to determine the spatial distribution in the present study.

3 Results and discussion

3.1 Regional sea level response to surface flux perturbations

In order to find the spatial pattern in the North Pacific, we illustrate the regional changes in DSL as deviations from the basin average in the upper panels of Fig. 2. In the faf-stress experiment, MIROC6 shows a DSL rise in the KE region due to a northward shift of the KE (Fig. 2a). This response is in good agreement with the Sverdrup transport caused by the additional wind stress perturbations (Fig. 1a). The wind-stress perturbation is related to the northward shift of the Aleutian Low, as

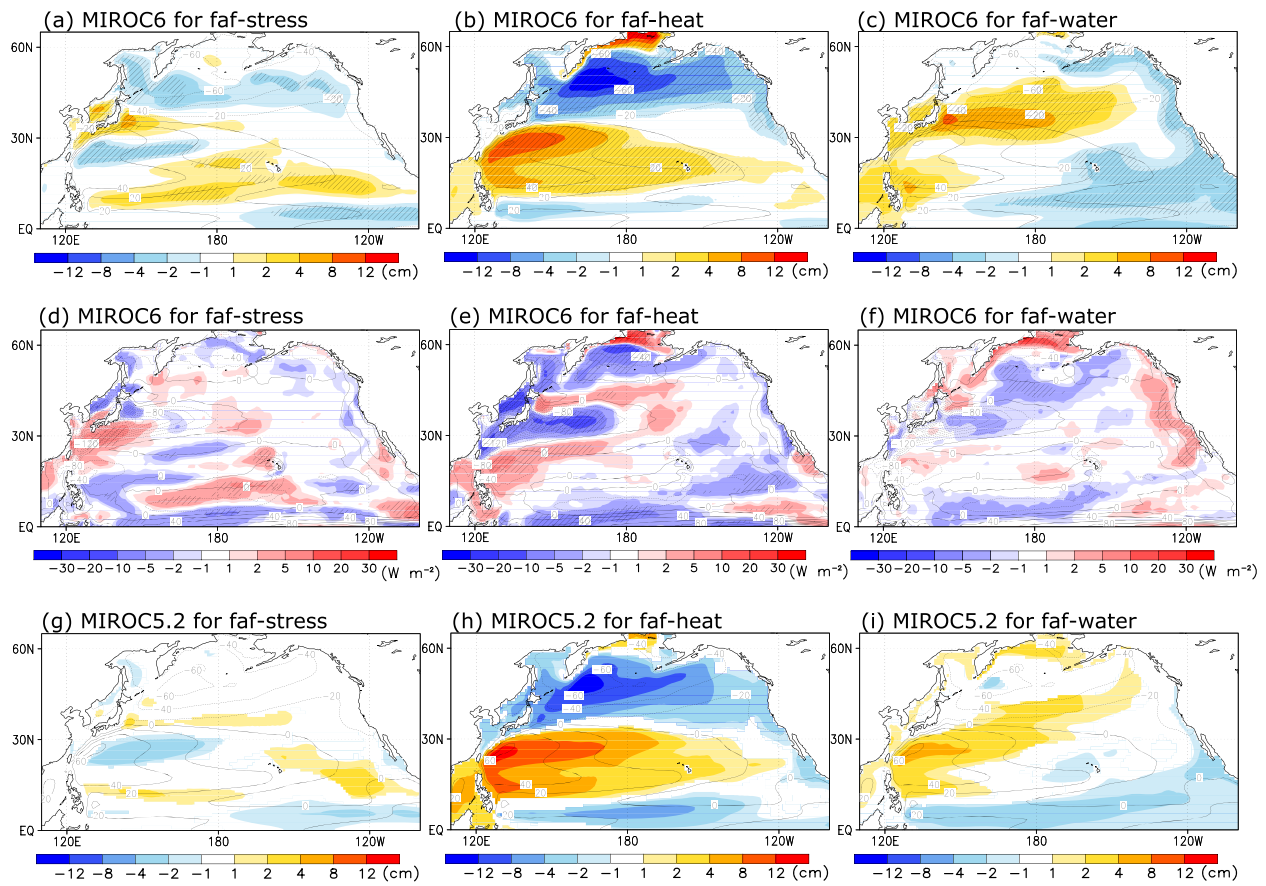

Fig. 2 Dynamic sea level changes (cm) for years 51–70 relative to piControl for **a** faf-stress, **b** faf-heat, and **c** faf-stress experiments of MIROC6. The contours in the upper panels indicate the climatological dynamic sea level in piControl. Regions with signals at a 90% confidence level are hatched. The middle panels show the heat flux change ΔQ_{SST} (Wm^{-2}) for years 1–70 relative to piControl for **d** faf-stress, **e** faf-heat, and **f** faf-stress experiments of MIROC6. The contour indicates the climatological net heat flux into the ocean in piControl. The lower panels (**g**–**i**) are same as the upper panels, but for the ensemble mean of three members of MIROC5.2. Areas in which the signs of the three members do not agree were masked out

mentioned by Sueyoshi and Yasuda (2012). Although a basin-scale DSL rise in the subtropical North Pacific is found in CMIP5-MME (Fig. 1d), this is not the case for the faf-stress experiment. Between 20° N and 30° N, the changes in the wind stress tend to suppress the DSL rise (Fig. 1a). The faf-stress experiment also shows that the DSL is depressed in the KE recirculation region to the south of 30° N.

The faf-heat experiment shows a significant increase in DSL in the recirculation region of the KE, where STMW is distributed (Fig. 2b). The spatial pattern is not consistent with the local heat input of the heat flux perturbation, which is relatively uniform in the subtropical gyre (Fig. 1b). The physical mechanism of this DSL is discussed later herein. The DSL change in the faf-water experiment (Fig. 2c) exhibits a basin-wide pattern similar to that in the Pacific Decadal Oscillation (e.g., Mantua et al. 1997; Yasuda and Sakurai 2006). However, this spatial pattern disappears in the following two decades. This may indicate that the warming signals and internal variability in the climate system are not sufficiently distinguished. The characteristic spatial pattern of the DSL changes seen in the faf-stress and the faf-heat experiments of MIROC6 are also found in the MIROC5.2 (Fig. 2g and h). In the faf-water experiment, however, MIROC5.2 shows a DSL rise in the KE recirculation, which differs from MIROC6.

The freshwater perturbations applied for the faf-water experiment show that the freshwater evaporates in the subtropical region and falls in the form of rain in the subarctic region (Fig. 1c). These changes are consistent with strengthening of the hydrological cycle over the twentieth and early twenty-first centuries (Durack et al. 2013). Although this could cause freshening of the STMWs and the DSL rise in the KE recirculation, the response is not robust across the models. Therefore, the results of the faf-water experiment will not be discussed further in the present study.

In the FAFMIP experiments, we used a climate model that considers air-sea coupled feedback processes that can occur in response to the SST changes. Therefore, the sum of the regional DSL changes resulting from individual experiments of faf-stress, faf-heat, and faf-water is not equal to that in the 1pct CO_2 experiment. The surface heat flux (Q) changes correspond to the SST changes (especially due to the changes in T_R for the faf-heat experiment). In the faf-stress experiment, the northward movement of the KE with a large amount of heat release causes anomalous heat absorption to the south of the KE and heat release to the north (Fig. 2d). In the faf-heat experiment, the heat release in the KE is increased relative to piControl (Fig. 2e). This is consistent with the enhancement of the subtropical gyre circulation, including the KE, and its heat transport. On the other hand, the net ocean heat absorption into the entire North Pacific is approximately the same in these experiments.

In order to investigate the time evolution of these DSL changes, we show the time series of the area-averaged DSL in the KE region (33° N–37° N, 140° E–150° E) and the KE recirculation region (20° N–35° N, 140° E–160° E) in order to determine the meridional shift of the KE and the strength of the recirculation gyre of the KE, respectively (upper panels in Fig. 3). The gray band in the figure indicates the width of the interannual variations in piControl. The range is estimated as $\pm Z S$, where S is the interannual standard deviation in piControl, and Z (1.96) is the 95th percentile of the normal distribution.

In the KE recirculation region, the faf-heat experiment exhibits a significant DSL rise, more than the amplitude of internal variability (red line in Fig. 3a). This signal appears clearly after about the 30th year and persists thereafter (dotted red line in Fig. 3a). Focusing on the KE, there are no significant changes beyond the width of interannual variations in piControl. However, looking at the difference in the mean over a longer time scale from the 20th year to the 90th year, the DSL of the faf-stress experiment becomes higher than in piControl by approximately 3 cm (dotted green line in Fig. 3b). This difference between the faf-stress and piControl is statistically significant at the 90% confidence level in the time mean over decades, as indicated by the hatched area in Fig. 2a. Similar DSL changes in the KE and the KE recirculation are observed in the ensemble mean of the three members of MIROC5.2 (Fig. 3e and f).

In order to understand the mechanisms of these DSL changes, we investigate the stream function of the Sverdrup transport derived from the wind stress change (including the wind stress perturbation for the faf-stress experiment). In the KE region, the variation in the DSL follows the changes in the Sverdrup transport stream function (Fig. 3d), suggesting that the wind stress change causes the northward shift of the KE. The correlation coefficient of the DSL change is approximately 0.76 with a 2-year lag. The time lag could be explained by the response time of ocean circulation to the wind stress change through the baroclinic Rossby wave propagation (Yasuda and Sakurai 2006). The DSL rise in the KE recirculation consists of the thermosteric sea level change (red line in Fig. 3c). On the other hand, the DSL change associated with the wind-driven Sverdrup transport stream function in this region is much smaller than that associated with the thermosteric component for time mean over decades (Fig. 3c). We describe the regional sea level growth caused by the heat flux perturbation in the next section.

3.2 Heat accumulation in the Kuroshio Extension recirculation gyre

The thermosteric sea level change $\Delta\eta_\theta$ and its components $\Delta\eta_{TR}$ and $\Delta\eta_{TA}$ in the faf-heat experiment and the thermosteric sea level change due to T_A ($\Delta\eta_{TA}$) in the

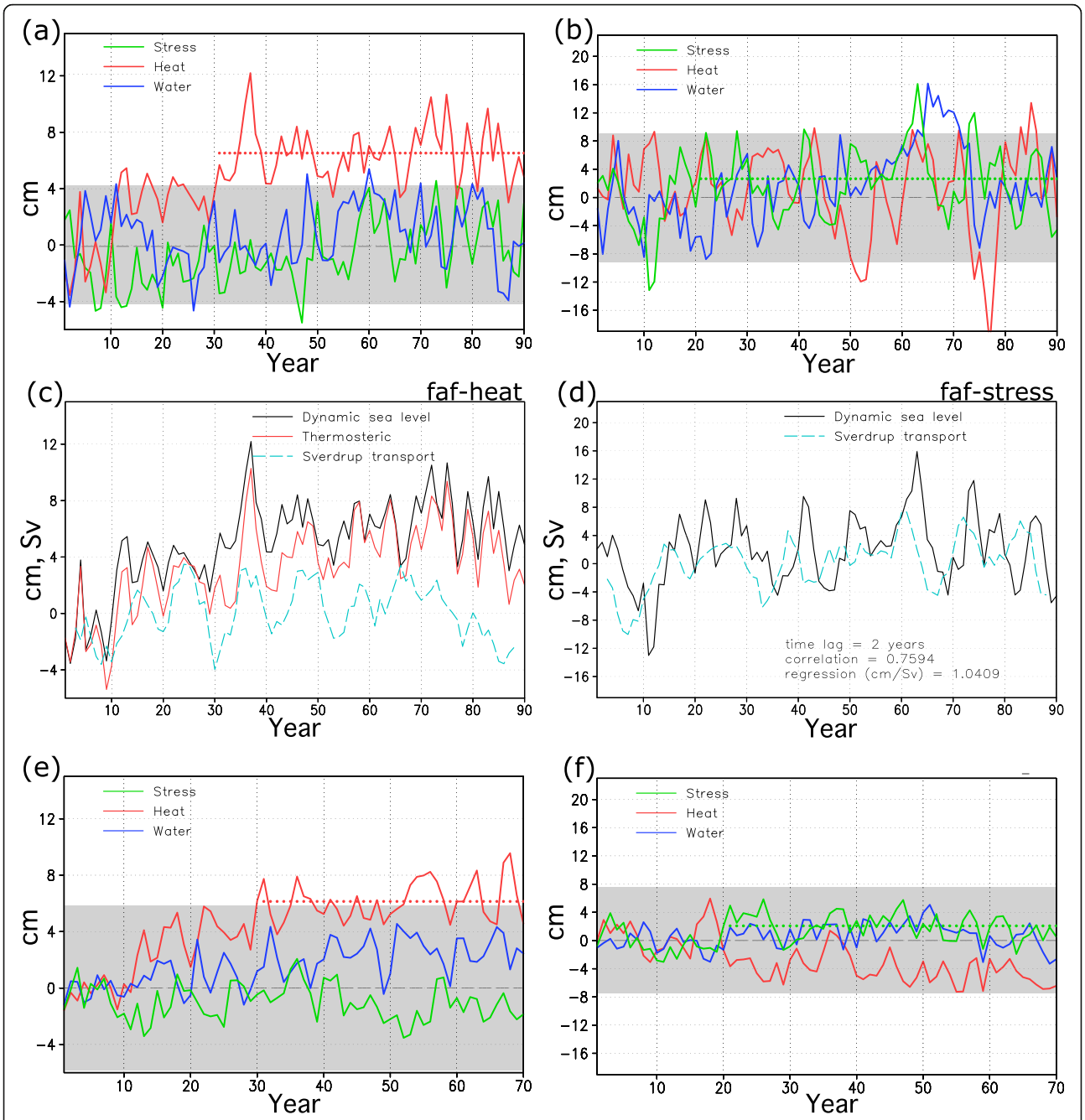

Fig. 3 Time series of DSL in **a** the KE recirculation (20° N–35° N, 140° E–160° E) and **b** KE (33° N–37° N, 140° E–150° E) for faf-stress experiment (green lines), faf-heat experiment (red lines), and faf-water experiment (blue lines). The red dotted line in **a** shows the time average of the faf-heat experiment between years 30 and 90 (6.5 cm). The green dotted line in **b** indicates the time average of the faf-stress experiment between years 20 and 90 (2.7 cm). The shaded areas in the upper panels indicate the range of piControl. **c** The DSL change (black line), the thermosteric sea level change (red line), and the Sverdrup transport stream function (dotted sky-blue line) in the KE recirculation for the faf-heat experiment. **d** The changes in the DSL (black line) and the Sverdrup transport stream function (dotted sky-blue line) in the KE for the faf-stress experiment. **e**, **f** Same as **a** and **b**, respectively, but for the ensemble mean of MIROC5.2. The red dotted line in **e** shows the time average of the faf-heat experiment between years 30 and 70 (6.1 cm). The green dotted line in **f** indicates the time average of the faf-stress experiment between years 20 and 70 (2.1 cm)

passive-heat experiment are shown in Fig. 4. In order to focus on these spatial distributions, we show the deviations from the North Pacific basin average. The DSL rise in the KE recirculation can be explained by the additional heat associated with global warming, suggesting the warming of STMW. However, the contribution of

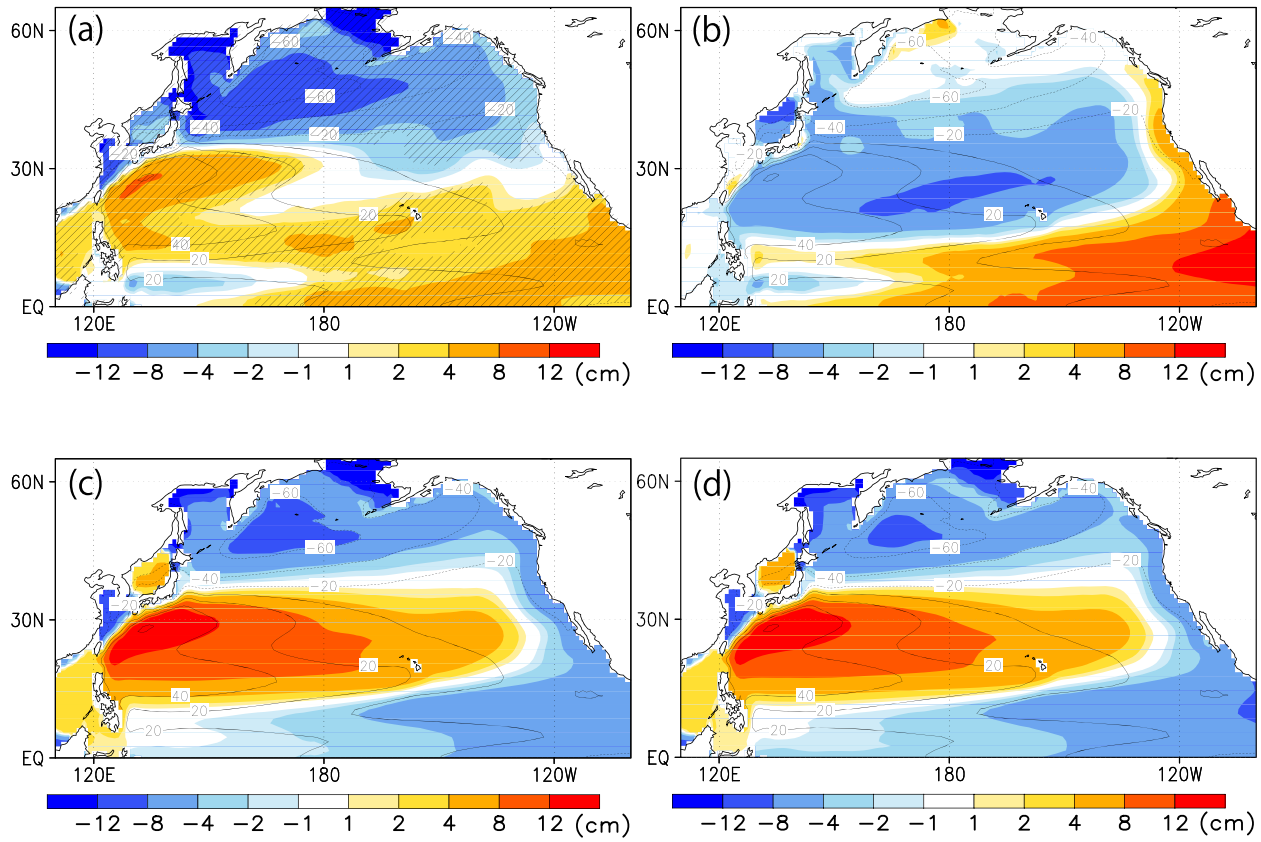

Fig. 4 **a** The thermosteric sea level change $\Delta\eta_\theta$ (cm), **b** thermosteric sea level change due to T_R ($\Delta\eta_{TR}$), and **c** thermosteric sea level change due to T_A ($\Delta\eta_{TA}$) for years 51–70 in the faf-heat experiment of MIROC6, and **d** the thermosteric sea level change due to T_A ($\Delta\eta_{TA}$) for years 51–70 in the passive-heat experiment of MIROC6. Note that deviations from the basin average in the North Pacific are depicted in the figures. Areas with signals at a 90% confidence level are hatched in **a**. Note that the basin average in the North Pacific is subtracted from the thermosteric sea level change at each grid. Contours indicate the climatological DSL in piControl

the T_R field is negative in this area (Fig. 4b). As a result, the thermosteric sea level rise (Fig. 4a) is smaller than that estimated from the T_A field (Fig. 4c).

The thermosteric sea level due to the T_A in the faf-heat experiment is in good agreement with that in the passive-heat experiment (Fig. 4d). We show the time march of T_A along 160° E for the faf-heat and the passive-heat experiments in Fig. 5. Both added heat tracers are subducted into the ocean subsurface to the south of 30° N and accumulated in the KE recirculation region, where STMW is distributed. The passive tracer does not affect the oceanic circulation. Therefore, these agreements indicate that heat transport by climatological mean currents largely determine the thermosteric rise in the Kuroshio recirculation under global warming.

We conducted the four additional faf-heat experiments with modified heat flux perturbations using MIROC5.2 in order to specify which areas of heat input contribute to the DSL rise in the KE recirculation. In these experiments, the experimental configurations are the same as the faf-heat experiment using MIROC5.2, but the heat flux perturbation is limited to the specific areas, namely, the subtropical gyre region (4° N–38° N, 100° E–100° W), the subpolar gyre region (38° N–64° N, 100° E–100° W), the southern part of the subtropical gyre (4° N–20° N, 130° E–130° W), and the areas excluding the Kuroshio and the KE recirculation region (20° N–35° N, 120° E–160° E). The net surface heat flux perturbations into the ocean in these regions are 96.2 TW, 37.8 TW, and 33.3 TW, and the remaining value excluding 13.8 TW from the whole heat flux, respectively. Each experiment is integrated for 70 years from the initial conditions taken from piControl of MIROC5.2, which are the same as that of the first member of the FAFMIP experiments in MIROC5.2.

In these experiments, heat accumulation is observed in the KE recirculation (i.e., STMW is warming), suggesting a thermosteric sea level rise, although the magnitude is different (Fig. 6). Applying heat flux perturbation to the global ocean, the thermosteric sea level increase due to

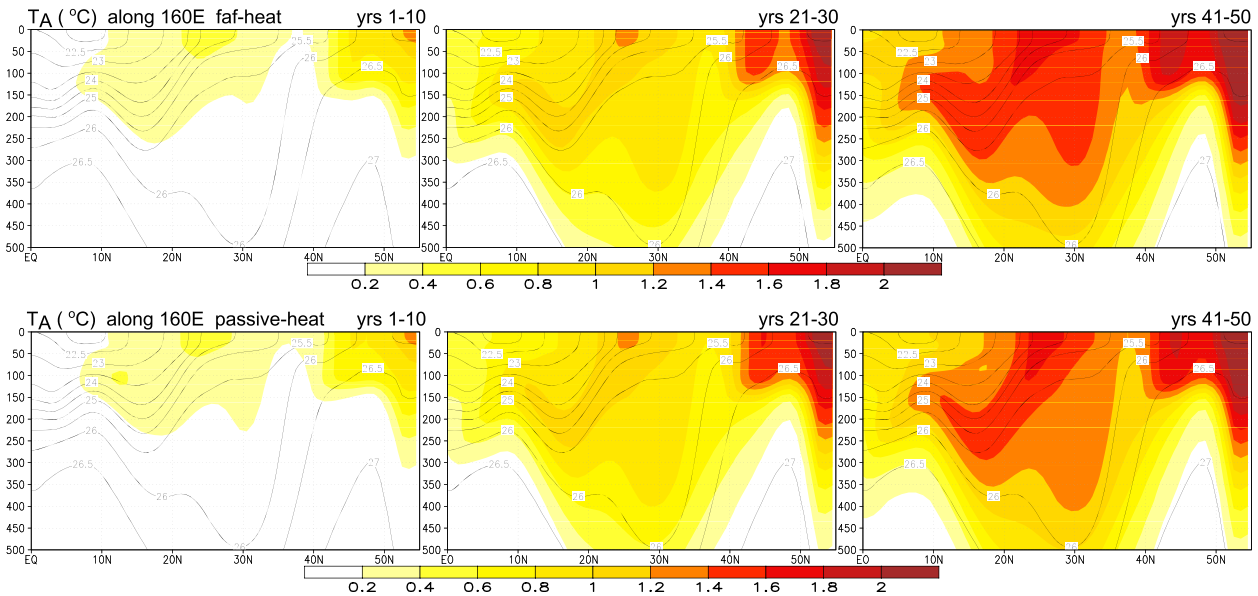

Fig. 5 Time march of latitude-depth sections of the added heat tracer T_A (°C) along 160° E for the first decade, the third decade, and the fifth decade for the faf-heat experiment (upper panels) and the passive-heat experiment (lower panels). Contours indicate the potential density (kg m^{-3}) in piControl

the additional heat tracer T_A ($\Delta\eta_{TA}$) is 25.06 cm (sum of the basin average and the deviation in the KE recirculation in Fig. 6) on the average of the final two decades of the 70 year-long integration in the KE recirculation region (20° N–35° N, 140° E–160° E). The added heat input in the subtropical and subpolar regions contributes to the increases in $\Delta\eta_{TA}$ in the KE recirculation of approximately 16.84 cm and 3.46 cm, respectively. The heat input in the subtropical gyre explains approximately 67.2% of the total sea level rise due to the added heat T_A

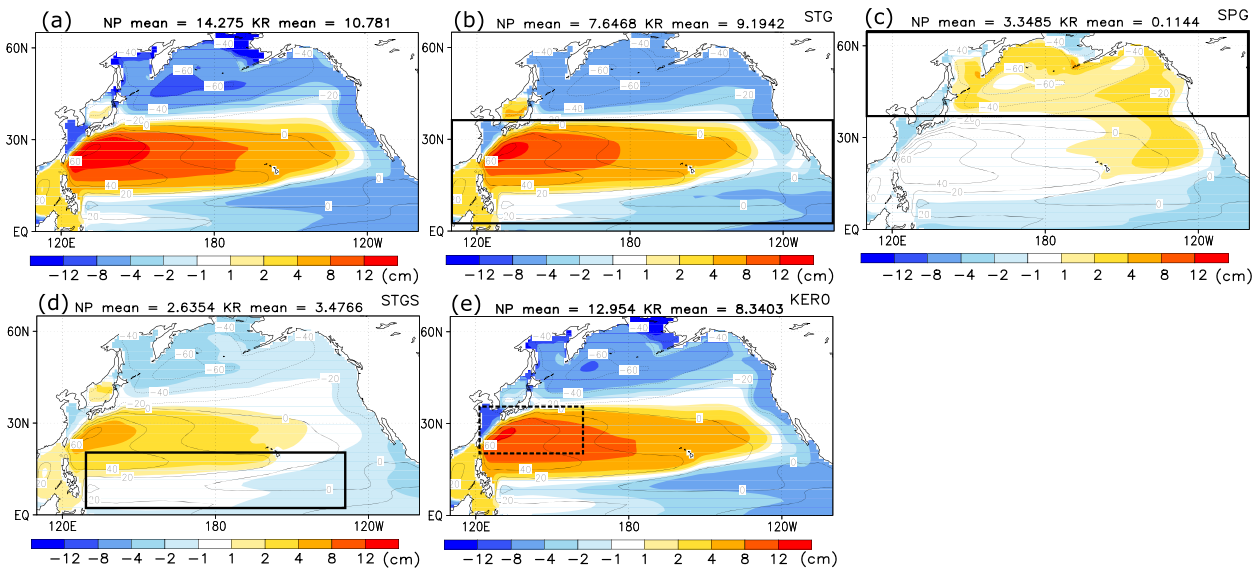

Fig. 6 Thermosteric sea level change (cm) due to the added heat T_A ($\Delta\eta_{TA}$) in the faf-heat experiment and in the case when the area to which the application of heat flux is limited to **b** the subtropical gyre region (4° N–38° N, 100° E–100° W), **c** the subpolar gyre region (38° N–64° N, 100° E–100° W), **d** the southern part of the subtropical gyre (4° N–20° N, 130° E–130° W), and **e** the area excluding the Kuroshio and the Kuroshio Extension recirculation (20° N–35° N, 120° E–160° E) for MIROC5.2. Note that the basin average in the North Pacific is subtracted at each grid. The numbers on each figure show the basin average of the North Pacific (NP mean) and the area average of the deviation in the Kuroshio Extension recirculation (KR mean). Contours indicate the climatological DSL in piControl. The solid boxes indicate the area given by heat flux perturbation (**b**, **c**), and the dotted box indicates the area excluding the heat flux perturbation (**e**)

in the KE recirculation region. Applying the heat flux perturbation to only the southern part of the subtropical gyre, the additional heat tracer increases by 6.11 cm, explaining 24.4% of the total rise. We have also estimated the thermosteric sea level rise ($\Delta\eta_\theta$) including the effects of T_R in Table 1. In the faf-heat experiment, the thermosteric sea level rise $\Delta\eta_\theta$ is 17.81 cm on average for the last two decades of the 70 year-long integration in the KE recirculation region. The changes in the redistributed heat T_R reduce the thermosteric sea level rise to approximately two-thirds of the increase due to T_A. Terada and Minobe (2018) found moderate correlation between the heat input to the south and southeast of Japan and the density decrease of STMW in the CMIP5 models. However, the additional faf-heat experiment that excludes the flux perturbation in the Kuroshio and the KE recirculation region (i.e., the south and southeast of Japan) can also explain 89% of the thermosteric sea level rise in the KE recirculation (Table 1). This means the heat absorption in this area does not fully explain the temperature rise of STMW and the related sea level rise. The results of the present study indicate that ocean heat flux in the broader field of the subtropical gyre is essential for heat accumulation in STMW.

4 Conclusions

We have estimated the contribution of ocean heat uptake to the DSL change in the western subtropical North Pacific following a set of climate model experiments designated in the FAFMIP protocol. Note that, unlike in previous studies, the surface heat flux changes under the global warming are explicitly given as a surface boundary condition.

The heat flux changes under global warming can lead to a continuous rise in sea level in the KE recirculation region due to the increase in temperature of STMW. The process of heat transfer into the subsurface that causes the warming of STMW is primarily determined by the climatological mean flow. This means that the thermosteric contribution due to local heat input cannot sufficiently reproduce the DSL change. The change in wind stress during warming contributes to the northward shift of the KE, but cannot be distinguished significantly from internal variations. The northward shift causes the heat input anomaly to the south and southeast of Japan (Fig. 2d), although the heat uptake is not sufficient to cause the DSL rise in the recirculation region of the KE. This means that the total heat uptake in the whole subtropical gyre causes the DSL rise in the KE recirculation.

Zhang et al. (2014) showed that a decrease in the DSL could have occurred associated with the spin-down of the subtropical gyre due to changes in the wind stress field. These responses are also found in the faf-stress experiment. The KE recirculation region defined in the present study corresponds to the northern part of the North Pacific subtropical gyre. The DSL change in the KE recirculation during global warming depends on whether the response to wind stresses or the contribution of the ocean heat uptake is dominant. Assuming that climatological mean currents determine the redistribution of surface heat input under the global warming, the model uncertainty in the future DSL change, a part of which is caused by thermosteric processes, could arise from differences in the representation of ocean climatology among climate models. In the future, we intend to compare the analysis of the present study with the results of the models participating in FAFMIP, to investigate the causes of variations in sea level change for each factor, and to clarify the uncertainty in future sea level change projections.

Table 1 Thermosteric sea level change ($\Delta\eta_\theta$) and $\Delta\eta_{TA}$ in the KE recirculation (20° N–35° N, 140° E–160° E) on average for the final two decades of the 70 year-long integration for (a) the faf-heat experiment and the four additional faf-heat experiments limiting the heat flux perturbation to the specific areas, (b) the subtropical gyre region (4° N–38° N, 100° E–100° W), (c) the subpolar gyre region (38° N–64° N, 100° E–100° W), (d) the southern part of the subtropical gyre (4° N–20° N, 130° E–130° W), and (e) the areas excluding the Kuroshio and the KE recirculation region (20° N–35° N, 120° E–160° E)

	$\Delta\eta_\theta$ (cm)		$\Delta\eta_{TA}$ (cm)	
(a) faf-heat	17.81	100%	25.06	100%
(b) STG	10.82	61%	16.84	67%
(c) SPG	1.95	11%	3.46	14%
(d) STGS	3.62	20%	6.11	24%
(e) Excluding KER	15.82	89%	21.29	85%

Acknowledgements
Model simulations were performed on the Earth Simulator at JAMSTEC. The authors would like to thank Shoshiro Minobe, Yoshiki Komuro, and Masahiro Watababe for their fruitful comments. The authors are much indebted to Koji Ogochi, Teruyuki Nishimura, Hiroaki Kanai, and Hiroshi Koyama for their long-term support in areas related to model development, source code optimization, and server administration.

Authors' contributions
TS proposed the topic, designed the study, conducted the model experiments presented in the paper, and wrote a large part of the paper. HT developed the model and supported the idealized experiments. TS and HT continuously discussed the results. All authors have read and approved the final manuscript.

Funding
This research was supported by the Integrated Research Program for Advancing Climate Models (TOUGOU program) of the Ministry of Education, Culture, Sports, Science and Technology (MEXT), Japan (JPMXD0717935457).

Availability of data and materials
The primary dataset supporting the conclusions of this article is available from the Earth System Grid Federation (ESGF). Contact the author for additional data sets.

Competing interests
The authors declare that they have no competing interest.

Received: 3 March 2020 Accepted: 16 October 2020
Published online: 09 November 2020

References

Bouttes N, Gregory JM, Kuhlbrodt T, Smith R (2014) The drivers of projected North Atlantic sea level change. Climate Dynamics *43*(5):1531–1544. https://doi.org/10.1007/s00382-013-1973-8

Cazenave A, Cozannet GL (2014) Sea level rise and its coastal impacts. Earth's Future. https://doi.org/10.1002/2013ef000188

Church JA, Clark PU, Cazenave A, Gregory JM, Jevrejeva S, Lever-mann A, Merri eld MA, Milne GA, Nerem RS, Nunn PD, Payne AJ, Pfeer WT, Stammer D, Unnikrishnan AS (2013a) Chapter 13: Sea level change. In: Stocker TF, Qin D, Plattner G-K, Tignor M, Allen SK, Boschung J, Nauels A, Xia Y, Bex V, Midgley PM (eds) Climate change 2013: the physical science basis. Contribution of Working Group I to the Fifth Assessment Report of the Intergovernmental Panel on Climate Change. Cambridge University Press, New York, pp 1137–1216. https://doi.org/10.1017/CBO9781107415315.026

Church JA, White NJ, Konikow LF, Domingues CM, Cogley JG, Rignot E, Gregory JM, van den Broeke MR, Monaghan AJ, Velicogna I (2013b) Correction to "Revisiting the Earth's sea-level and energy budgets from 1961 to 2008". Geophys Res Lett. 40(15):4066–4066. https://doi.org/10.1002/grl.50752

Durack PJ, Wijffels SE, Boyer TP (2013) Long-term salinity changes and implications for the global water cycle. In: International Geophysics, vol 103, pp 727–757. Academic Press. https://doi.org/10.1016/B978-0-12-391851-2.00028-3

Gregory JM, Bouttes N, Griffies SM, Haak H, Hurlin WJ, Jungclaus J, Kelley M, Lee W, Marshall J, Romanou A, Saenko O, Stammer D, Winton M (2016) The Flux-Anomaly-Forced Model Intercomparison Project (FAFMIP) contribution to CMIP6: investigation of sea-level and ocean climate change in response to CO2 forcing. Geoscientific Model Dev *9*(11):3993–4017. https://doi.org/10.5194/gmd-9-3993-2016

Griffies SM, Danabasoglu G, Durack PJ, Adcroft AJ, Balaji V, Böning CW, Chassignet E, Curchitser E, Deshayes J, Drange H, Fox-Kemper B, Gleckler P, Gregory J, Haak H, Hallberg R, Heimbach P, Hewitt H, Holland D, Ilyina T, Jungclaus J, Komuro Y, Krasting J, Large W, Marsland S, Masina S, McDougall T, George Nurser A, Orr J, Pirani A, Qiao F, Stouffer R, Taylor K, Treguier A, Tsujino H, Uotila P, Valdivieso M, Wang Q, Winton M, Yeager S (2016) OMIP contribution to CMIP6: experimental and diagnostic protocol for the physical component of the Ocean Model Intercomparison Project. Geoscientific Model Dev 9:3231–3296. https://doi.org/10.5194/gmd-9-3231-2016

Levitus S, Antonov JI, Boyer TP, Baranova OK, Garcia HE, Locarnini RA, Mishonov AV, Reagan JR, Seidov D, Yarosh ES, Zweng MM (2012) World ocean heat content and thermosteric sea level change (0-2000 m), 1955-2010. Geophys Res Lett 39(10). https://doi.org/10.1029/2012GL051106

Liu Z-J, Minobe S, Sasaki YN, Terada M (2016) Dynamical downscaling of future sea-level change in the western North Pacific using ROMS. J Oceanogr 72:905–922. https://doi.org/10.1007/s10872-016-0390-0

Lowe JA, Gregory JM (2006) Understanding projections of sea level rise in a Hadley Centre coupled climate model. J Geophys Res 111:C11014. https://doi.org/10.1029/2005JC003421

Mantua NJ, Hare SR, Zhang Y, Wallace JM, Francis RC (1997) A Pacific interdecadal climate oscillation with impacts on salmon production. Bull Am Meteorol Soc *78*:1069–1079

Sueyoshi M, Yasuda T (2012) Inter-model variability of projected sea level changes in the western North Pacific in CMIP3 coupled climate models. J Oceanogr *68*:533–543. https://doi.org/10.1007/s10872-012-0117-9

Suzuki T, Ishii M (2011) Regional distribution of sea level changes resulting from enhanced greenhouse warming in the Model for Interdisciplinary Research on Climate version 3.2. Geophys Res Lett 38:L02601. https://doi.org/10.1029/2010GL045693

Tatebe H, Ogura T, Nitta T, Komuro Y, Ogochi K, Takemura T, Sudo K, Sekiguchi M, Abe M, Saito F, Chikira M, Watanabe S, Mori M, Hirota N, Kawatani Y, Mochizuki T, Yoshimura K, Takata K, O'ishi R, Yamazaki D, Suzuki T, Kurogi M, Kataoka T, Watanabe M, Kimoto M (2019) Description and basic evaluation of simulated mean state, internal variability, and climate sensitivity in MIROC6. Geoscientific Model Dev *12*(7):2727–2765. https://doi.org/10.5194/gmd-12-2727-2019

Tatebe H, Tanaka Y, Komuro Y, Hasumi H (2018) Impact of deep ocean mixing on the climatic mean state in the Southern Ocean. Sci Rep. https://doi.org/10.1038/s41598-018-32768-6

Terada M, Minobe S (2018) Projected sea level rise, gyre circulation and water mass formation in the western North Pacific: CMIP5 inter-model analysis. Climate Dynamics *50*(11–12):4767–4782. https://doi.org/10.1007/s00382-017-3902-8

Willis JK, Church JA (2012) Climate change. Regional sea-level projection. Science (New York, N.Y.) 336(6081):550–551. https://doi.org/10.1126/science.1220366

Yasuda T, Sakurai K (2006) Interdecadal variability of the sea surface height around Japan. Geophys Res Lett. 33:L01605. https://doi.org/10.1029/2005GL024920

Yin J (2012) Century to multi-century sea level rise projections from CMIP5 models. Geophys Res Lett 39:L17709. https://doi.org/10.1029/2012GL052947

Zhang X, Church JA, Platten SM, Monselesan D (2014) Projection of subtropical gyre circulation and associated sea level changes in the Pacific based on CMIP3 climate models. Climate Dyn 43:131–144. https://doi.org/10.1007/s00382-013-1902-x

Publisher's Note

Springer Nature remains neutral with regard to jurisdictional claims in published maps and institutional affiliations.

Submit your manuscript to a SpringerOpen journal and benefit from:

► Convenient online submission
► Rigorous peer review
► Open access: articles freely available online
► High visibility within the field
► Retaining the copyright to your article

Submit your next manuscript at ► springeropen.com